



Research Paper

CO_x-free hydrogen production via decomposition of ammonia over Cu–Zn-based heterogeneous catalysts and their activity/stability

Špela Hajduk^a, Venkata D.B.C. Dasireddy^b, Blaž Likozar^b, Goran Dražić^a, Zorica Crnjak Orel^{a,*}

^a Department of Materials Chemistry, National Institute of Chemistry, Hajdrihova 19, SI-1001 Ljubljana, Slovenia

^b Department of Catalysis and Chemical Reaction Engineering, National Institute of Chemistry, Hajdrihova 19, SI-1001 Ljubljana, Slovenia

ARTICLE INFO

Article history:

Received 31 January 2017
Received in revised form 7 April 2017
Accepted 10 April 2017
Available online 12 April 2017

Keywords:

NH₃ conversion
Apparent activation energy
H₂ selectivity
Chemical hydrogen storage
Copper–Zinc/Alumina
Non-noble metal catalysis

ABSTRACT

Cu–Zn mixed metal oxides were synthesized with a modified citrate method, supported on an Al₂O₃ substrate, and tested for ammonia decomposition process to attain a high-purity hydrogen generation for fuel cells. Alumina-supported catalytic materials prepared by wet impregnation technique exhibited the highest surface copper species dispersion along with an increase in distributed acidic and basic sites. TPD studies using NH₃ and CO₂ revealed the presence of the Lewis and Brønsted acidity and basicity. SEM demonstrated a uniform particle distribution and morphology, regardless of Cu/Zn ratio. Cu/ZnO/Al₂O₃ exhibited a superior conversion activity when compared to neat Cu–Zn, which may be due to an improved Cu–Zn synergistic effect, a smaller average bimetallic nanoparticle size, and moderate acid–base characteristics. TEM micrographs confirmed the round-shaped metallic particles, ranging up to 7 nm in diameter and comprising both active copper oxide phases (Cu¹⁺ and Cu²⁺), further investigated by EELS spectroscopy, as well as by XPS analysis. With reactions resulting in an effective first-order turnover (rate-determining step limitation), the apparent activation energies of (50–80) ± 5 kJ mol⁻¹ were estimated in between 450 and 600 °C which is in agreement with other commercial catalysts. All fabricated bi-functional catalysts exhibited a high long-term stability and hydrogen productivity; nonetheless, comprised no critical scarce raw resources (e.g. platinum-group metals), which is appealing for emerging chemically-bonded H₂ storage and release be it in relation to production only (electrolysis) or with consumption (regenerative fuel cells).

© 2017 Elsevier B.V. All rights reserved.

1. Introduction

Ammonia is a second most widely produced chemical in the world (after sulphuric acid), with over 100 million tons per year being transported [1,2]. It is a promising hydrogen (H₂) carrier because of many advantages [3,4]. The main reason is the high H₂ content of 17.8 mass% in NH₃ [1,5]. One of the crucial reasons are also infrastructures that produce, store and carry NH₃ have been universally established because huge amounts of NH₃ are now produced as fertilizer by the Haber-Bosch process. Therefore, after H₂ release from NH₃ is not necessary to collect nitrogen (N₂) as the by-product because it can be released to the air [5–7]. Ammonia is a carbon-free fuel and its decomposition to hydrogen does not produce any carbon monoxide or carbon dioxide [8,9]. Hydrogen is the cleanest fuel ever known, and despite being the most attrac-

tive fuel for polymer electrolyte membrane fuel cells (PEMFCs) [9] the storage of hydrogen is still a limiting factor which entails safety risks, non-competitive overall efficiency and lower volumetric density compared to the other fuels [2,3]. The use of ammonia as a hydrogen carrier appears to be a better choice in comparison to hydrogen generated from carbonaceous substances (e.g. methane or methanol), as there is no CO_x generation and the unconverted NH₃ can be reduced to less than 2 × 10⁻⁵ mol% level by means of a suitable absorber [10,11]. On the other hand, the hydrogen storage capacity and energy density (3000 Wh/kg) of ammonia are higher than those of methanol or other fuels. The huge advantage from an economics standpoint it has been reported, that NH₃ decomposition is a more economical process for hydrogen generation compared to methanol reforming [10–12].

From the literature [13], it can be seen that in the optimal ammonia decomposition process it is necessary to grade the reactor with catalysts that have different nitrogen binding energies, as is also the case in the optimal ammonia synthesis process. It is demonstrated that the optimal catalyst for ammonia decomposition is

* Corresponding author.

E-mail address: zorica.crnjak.orel@ki.si (Z.C. Orel).

never the optimal catalyst for ammonia synthesis. Despite all the developments, the absence of an efficient and low-cost method for the ammonia decomposition into hydrogen remains a challenge [2,3,9].

Some studies considering catalysts to decompose NH₃ and generate H₂ have been carried out [1,5]. Much research effort has been mainly devoted to group 8 and 9 metals (Ru, Ir, Co, Fe and Rh) or metal nitrides/carbides (MoN_x, VN_x, VC_x, MoC_x, etc.) [12,14–17]. For ammonia decomposition reaction it has been found that ruthenium (Ru) is the most active catalyst [10,18]. However, Ru is a scarce metal with a very high price for practical commercial purposes. To overcome this problem, cheaper materials have been proposed through theoretical studies and experimental screening, especially alloys [9,13]. Transition metals such as Fe, Cu, Co, and Ni are promising candidates for this reaction [15,16]. The Ni–Pt–Pt bimetallic surface was predicted to be very active for the ammonia decomposition reaction [19]. The studies indicate that a Ni–Pt–Pt catalyst may be more active than Ru-based on a lower nitrogen desorption temperature and a remarkably low dehydrogenation barrier, both of which were determined to be kinetically significant reaction steps. In this study, we present Cu-Zn mixed oxides as superior catalysts obtained by citrate method. Previously, we have reported about copper-zinc co-precipitation method where the average size of particles decreases with increasing the concentration of added copper ion solution. Also, we demonstrated that presence of urea changes the formation of Cu-Zn particles in terms of particle structure and size [20,21]. In this paper, we present the simple method to obtain homogeneous copper-zinc particles. Mixed oxides were synthesized by contacting the metal cations with citrate ion. The citrate-gel method allows preparation of highly dispersed mixed oxides [22,23]. The method involves linking of various mixed ions with citrate that due to the three-ligand nature of citrate forms a transparent three-dimensional network upon drying (gel). The pyrolysis of this gel results in a homogeneously mixed oxides [22]. The Cu-Zn catalysts have been widely used for other applications e.g. water-gas shift reactions (WGSR) or methanol synthesis. The so-called synergy originates from the contacts between Cu and ZnO, created during the reduction step of a catalyst [24,25]. In our case, the synergistic effect could enhance the interaction between the active centers and the catalyst support [26]. This leads to increased basic activity and brings the whole reaction to lower temperatures [7]. Tseng et al. [27,28] reported that for Cu/Zn catalysts, a higher Cu:Zn ratio causes an improved dispersion of surface Cu species. Cu/Zn materials, prepared through a poly-alcohol method, exhibited a lower Cu particle size and reduction/oxidation efficiency of Cu/Zn.

The importance of optimizing ammonia decomposition catalysts towards a more practical application is elucidated in the literature [9]. For a large scale production, the incipient wetness impregnation (IWI), also called capillary impregnation is considered the most advantageous method, owing to its low-cost, simplicity and ease of up-scaling [2,3]. A good support should at least possess the properties of (i) being stable under reaction conditions, and (ii) having a high specific surface area (SSA) [10]. Different supported metal catalyst systems have been examined for ammonia decomposition including a variety of supports such as Al₂O₃, SiO₂, TiO₂, ZrO₂, mesoporous and microporous materials, activated carbon, multi-walled carbon nanotubes (MWCNTs) etc. [14–16,29,30]. In this study, we present a novel synthesis route of a Cu-Zn/Al₂O₃ catalyst. This method has the advantage of low cost and relative simplicity. Copper-based materials are highly conductive, have a high SSA, and are promising in ammonia decomposition reaction for H₂ production. Zinc is low-cost semiconducting material as well and there is no published study on Cu-Zn mixed oxides as a promising alternative to replace expensive ruthenium-based catalysts for a real scale application of hydrogen

generation by ammonia decomposition. In this paper, the ammonia decomposition studies on multi-component mixed oxides and alumina supported Cu-Zn based catalysts were done.

2. Experimental

2.1. Catalyst preparation

Cu-Zn mixed oxides were synthesized from nitrate precursors by contacting the metal cations with citrate ion. Zinc and copper salts were prepared separately with modified citrate method in two steps [31]. First, 1.2 mL of 65% HNO₃ (Merck) was slowly added to 0.613 g of Zn²⁺ ions ((Zn(NO₃)₂ × 6H₂O, Aldrich, 99 mol%) in 4 mL of Milli-Q water (the resistance of 18.2 MΩ). The solution was marked as A. Solution B consisted of 0.8 g of citric acid (C₆H₈O₇ × H₂O; Kemika; ≥ 99.5 mol%), 2 mL of ethanol (C₂H₅OH; Sigma-Aldrich; ≥ 99.8 mol%) and 0.8 mL of Triton X-100 (Sigma-Aldrich). Both solutions were treated with ultrasound separately for 15 min and then stirred using a magnetic bar (400 rpm) at room temperature to ensure complete solubility. Then solution B was drop-wise added to the solution A and final solution C was stirred for 3 h under the conditions mentioned above. After that, the mixture (C) was aged for 24 h. To obtain a copper salt, the same amounts of the mentioned chemicals were used, but instead of zinc precursor, 0.375 g of copper nitrate (Cu(NO₃)₂ × H₂O; Aldrich; 99.999 mol%) was utilized. Then the metal oxides mixtures were prepared in molar ratios Zn/Cu (1:2 and 2:1) followed by increasing the pH up to 4.0–4.3 with ethanol to equalize metal oxides charges (CAT1 and CAT2). To ensure slow evaporation of ethanol the samples were heated in air in the following order – first at 40 °C for 1 h, then at 80 °C for 1 h and finally at 90 °C overnight. After that, the samples were treated at 400 °C for 4 h under continuous airflow (150 mL min⁻¹).

To enhance the catalytic activity of catalyst we added alumina to Cu-Zn metal oxides in two ways. Firstly, alumina sol-gel was prepared using the same sol-gel methodology, as mentioned above that is, utilizing 0.750 g of Al³⁺ ((Al(NO₃)₃ × 9H₂O; Sigma-Aldrich; 99.997 mol%). Afterward, metal oxide mixtures following two molar ratios (Zn/Cu/Al of 1:2:0.5 and 2:1:0.5) were prepared. Then the pH to c. 4.3 was increased, the samples were heated up in the air and treated in the same way like in above-mentioned procedure. Those samples are marked as CAT3 and CAT4. In a second way, we deposited alumina with wet impregnation method on bare samples CAT1 and CAT2. Alumina deposited on Cu-Zn alloy of different ratios is described in the following sentences. 100 mL of deionized water was added to a 250 mL beaker containing 4.0 g of γ-alumina under steady stirring (300 rpm). Consecutively, an appropriate predetermined amount of copper and zinc oxides (20 wt.%) was added, and the mixture was stirred for 5 h at the temperature of 70 °C. The paste obtained was dried overnight at 90 °C and then subjected to the calcination at 400 °C for 4 h under continuous airflow (150 mL min⁻¹) (samples CAT1/Al₂O₃, CAT2/Al₂O₃).

2.2. Catalyst characterisation

Brunauer–Emmett–Teller (BET) surface area and pore volume studies were carried out by firstly degassing the catalysts under the N₂ flow for 4 h at 200 °C using the Micrometrics FlowPrep 060. The degassed samples were analyzed in the Micrometrics ASAP 2020 multi-point BET surface area analyzer. X-ray diffraction (XRD) analysis was carried out in the Siemens D5000 apparatus, equipped with CuKα (40 kV; 30 mA) non-monochromatic radiation (the wavelength of 15.406 nm). The intensity was obtained by scanning from 5° to 60° (2θ angle range). Diffraction patterns were collected in stepwise increments of 0.04° at an acquisition

time of 1 s. Temperature-programmed desorption (TPD) runs were carried out using the Micromeritics Autochem II Chemisorption Analyzer. After reduction, the catalysts were pre-treated at 350 °C under the stream of helium for 60 min. The temperature was subsequently decreased to 80 °C. The appropriate gaseous mixture selected was passed over the catalysts (10 mol% CO in He/4.9 mol% H₂ in Ar) at the flow rate of 30 mL min⁻¹ for 60 min. The excess gas was removed by purging with helium for 30 min. The temperature was consequently gradually raised to 900 °C by ramping at 10 K min⁻¹ under the flow of helium, and the desorption data of CO or H₂ was recorded. Temperature-programmed reduction (TPR) was also performed using the Micromeritics Autochem II Chemisorption Analyzer. Prior to the reduction of a sample using the TPR, the catalysts were pre-treated by heating in the stream of argon (30 mL min⁻¹) at 400 °C for 30 min and subsequently cooled to 80 °C. Thereafter, the 4.9 mol% hydrogen in argon was used as the reducing agent at the flow rate of 30 mL min⁻¹. Samples were analyzed from the ambient temperature (25 °C) to 950 °C using the ramp rate of 10 °C min⁻¹.

The TPD for acidity/basicity determination was carried out using the Micromeritics Autochem II Chemisorption Analyzer as well. After reduction, the catalysts were pre-treated at 350 °C under the stream of helium for 60 min. The temperature was consequently decreased to 80 °C. Appropriate pre-chosen gas was passed over the catalysts (9.8 mol% NH₃ in He, 10 mol% CO₂ in He, or 4.9 mol% H₂ in Ar) at the flow rate of 30 mL min⁻¹ for 60 min. The excess gas was removed by purging with helium for 30 min. The temperature was thereafter gradually raised to 900 °C by ramping at 10 °C min⁻¹ under the flow of helium, wherein the desorption data of NH₃, CO₂ or H₂ was recorded.

The dispersion of Cu was measured by using dissociative N₂O chemisorption. The amount of the consumed hydrogen in the first temperature-programmed reduction was denoted as X. Subsequently, catalyst beds were purged with a highly pure He (99.99 mol%; 30 mL min⁻¹) and cooled to 50 °C. Following this, 10 mol% N₂O (in He) mixture with the flow rate of 50 mL min⁻¹ was introduced to the catalyst bed at 50 °C for 10 min to perform the dissociative adsorption and corresponding oxidation of Cu⁰ surface to Cu₂O. In order to remove excess oxidant, the samples were again flushed with a highly pure He (30 mL min⁻¹) and cooled to the ambient temperature (25 °C) under the same atmosphere. As the signal baseline stabilized, the second temperature-programmed reduction was performed on the samples. The amount of the consumed hydrogen in the second temperature-programmed reduction was denoted as Y. The dispersion of Cu was calculated according to the literature correlations [32,33].

Surface morphology for the supported catalysts was imaged using a Model Supra VP-35 field emission scanning electron microscope (SEM) with an accelerating voltage of 1 kV (Carl Zeiss). The elemental mappings, presented herein, were attained with the acceleration voltage of 20 kV, the aperture of 60 μm, and the gun-to-sample distance of 8 mm.

Transmission electron microscopy (TEM), scanning transmission electron microscopy (STEM) and electron energy loss spectroscopy (EELS) were performed on Jeol ARM 200 CF atomic resolution STEM with probe Cs corrector. For chemical analysis, Dual EELS Quantum ER system from Gatan and Jeol Centrino EDXS system with 100 mm² solid-state detectors were used. For TEM sample preparation powder samples were mixed with ethanol and a drop of suspension was placed on lacy carbon-coated Ni grids.

The x-ray photoelectron spectroscopy (XPS or ESCA) analyses were carried out on the PHI-TFA XPS spectrometer produced by Physical Electronics Inc. Samples were placed on a sample holder and introduced in an ultra-high vacuum spectrometer. The analyzed area was 0.4 mm in diameter and the analyzed depth of about 3–5 nm; this high surface sensitivity is a general characteristic of

the XPS method. Sample surfaces were excited by X-ray radiation from monochromatic Al source at the photon energy of 1486.6 eV. The high-energy resolution spectra were acquired by the energy analyzer operating at the resolution of approximately 0.6 eV and pass energy of 29 eV. During data processing, the spectra from the surface were aligned by setting the C 1s peak at 285.0 eV, characteristic for C–C bonds. The accuracy of binding energies was approximately ±0.3 eV. Quantification of surface composition was performed from XPS peak intensities taking into account relative sensitivity factors provided by the instrument manufacturer.

2.3. Catalytic testing

The ammonia decomposition reaction was done using a U-shaped quartz tube reactor. A 0.2 g of catalyst was packed in between the glass wool. Prior to the reaction, the catalyst was reduced with hydrogen in flowing argon (4.9% H₂ in He) at a total flow rate of 50 mL/min at a temperature of 600 °C for one hour. Then the samples were cooled down to the desired reaction temperature in the range of 300–600 °C under He flow and then the flow was changed to 9.8% NH₃ in He gas. The gas hourly space velocity was maintained as 15,000 h⁻¹. Decomposition of ammonia was carried out on individual γ-alumina support and empty quartz tube at different temperatures and the reaction conditions were maintained similar to those employed for the decomposition on prepared catalysts. The outlet gasses including ammonia, nitrogen, and hydrogen were analyzed by online quadrupole mass spectrometry (MS). The signals in the MS are calibrated with different mole fractions of ammonia, hydrogen, and nitrogen in order to determine the mole composition of gasses in the outflow. The NH₃ conversion was calculated from the mole fraction of H₂ (y_{H₂}) in the products according to the following equation [34,35]:

$$X_{\text{NH}_3} = \frac{2y_{\text{H}_2}}{3 - 2y_{\text{H}_2}} \quad (1)$$

Surface activity was also expressed in terms of the turnover frequency (TOF) of ammonia decomposition, which is significant for comparative purposes. TOF, also called turnover number, is defined as the molecules reacting per an active site in a time unit. The number of the reacting molecules of ammonia in a time unit was calculated using the conversion and the flow rate of ammonia at a corresponding reaction temperature and the available number of Cu/Zn active sites on a particular catalyst, which could be obtained from the dispersion of Cu/Zn atoms, measured from N₂O chemisorption [12,25].

3. Results and discussion

The BET surface areas, measured by the physical nitrogen adsorption for all of the samples, are presented in Table 1. The specific surface area of neat Al₂O₃ support was found to be 241 m²/g. However, BET surface area decreased with the presence of copper and zinc, and the latter might be due to the blocking of the pores of the support by crystallites of metal oxide, as evidenced by XRD and pore-size distribution measurements. The total pore volume also followed the decreasing trend, as the surface area was found to decrease with an increase of copper loading. The N₂ adsorption–desorption isotherms of the prepared catalysts can be categorized as the type IV isotherms, with a distinct hysteresis loop, observed in the range of 0.45–0.8 [36]. The pore-size distribution, calculated from desorption counterpart using Barrett–Joyner–Halenda (BJH) method, showed a dominant peak in the mesoporous range.

For a more precise determination of the dispersion of Cu species, the chemisorption of N₂O on the catalysts was carried out. It

Table 1

Particulate properties of prepared catalysts.

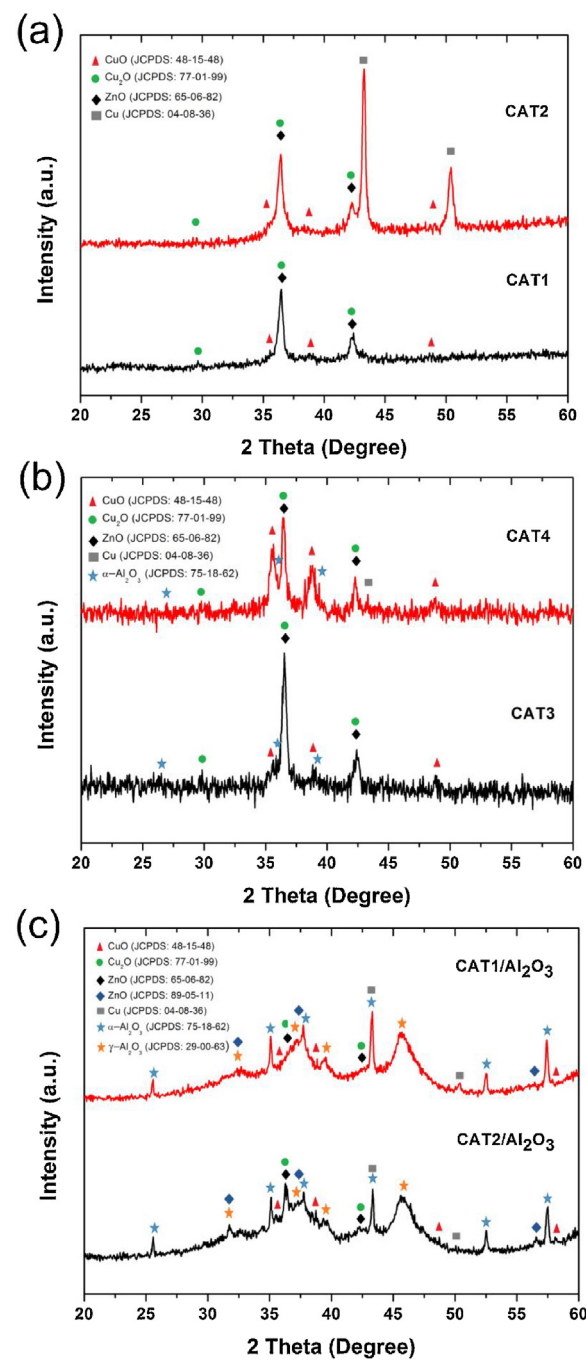
Catalyst	Cu/Zn/Al Composition (mol/mol/mol)	Surface Area (m^2/g) ^a	Pore volume (cm^3/g)	Metal dispersion (%) ^b	Crystallite size (nm) ^c
CAT1	1/2/0	9.8	0.07	5.1	21
CAT2	2/1/0	7.5	0.06	3.4	19
CAT3	1/2/0.5	18.0	0.09	10.8	17
CAT4	2/1/0.5	22	0.09	16.7	15
CAT1/ Al_2O_3	1/2/0.5	43.7	0.12	41.7	10
CAT2/ Al_2O_3	2/1/0.5	48.6	0.13	43.2	9

^a N₂ physisorption.^b N₂O chemisorption.^c Powder XRD.

can be seen that the both alumina supported catalysts, prepared by wet impregnation, exhibited the highest dispersion of copper species, which was as high in the range of 40 and 44 %, and that the dispersion of Cu species rose in the following order: CAT2/ Al_2O_3 > CAT1/ Al_2O_3 > CAT4 > CAT3. The catalysts with low zinc showed a lower dispersion compared to the copper analogues. Upon considering all catalysts, the catalysts prepared supported on alumina, showed a higher dispersion with regard to the ones, obtained by wet impregnation method. In general, with support results in a high dispersion and smaller particles as prepared in wet impregnation, as also evidenced by the pertinent literature [37,38].

XRD patterns of pristine mixed metal oxides (CAT1 and CAT2) on Fig. 1a show sharp peaks of cubic zinc oxide crystal phase (JCPDS: 65-06-82) with significant peaks for (111) and (200) plane. Both copper oxide phases (CuO and Cu₂O) can be observed (JCPDS: 48-15-48; JCPDS: 77-01-99), while the metal copper phase is present only at sample CAT2 assuming due to the higher ratio of copper to zinc (2 parts of copper and 1 part of zinc) in comparison with sample CAT1. Modified samples with alumina (CAT3 and CAT4) showed alumina phases (Fig. 1b) as we expected. In this case, the amount of alumina [39,40] is very low and hence the peaks are detected as very small. At these samples, α -alumina phase (JCPDS: 75-18-62) with d-spacing values of 2.55 Å and 2.38 Å (Table S1) for planes (104) and (110) is determined probably due to the lower temperature of the synthesis in comparison with alumina supported samples CAT1/ Al_2O_3 and CAT2/ Al_2O_3 . The samples are less crystalline from pristine metal oxides. The XRD profiles of alumina (Al_2O_3)-supported catalysts (samples CAT1/ Al_2O_3 and CAT2/ Al_2O_3) shown in Fig. 1c indicating the typical diffraction peaks with d-spacings of 2.39 Å and 2.28 Å indicated for (311) and (222) planes that can be assigned to cubic γ - Al_2O_3 (JCPDS: 29-00-63). Obtained d-spacing values for all catalysts are given in Supplementary Information (Table S1, S2, S3) Gamma alumina phase besides alpha alumina phase could appear due to the increased temperature of the synthesis as we mentioned before. Broad peaks observed for alumina-based supported catalysts, suggesting that the alumina-based materials contain dispersed particles of a finer nature and a less degeneracy in their crystallites than the other samples [41,42]. The diffraction peaks of samples CAT1/ Al_2O_3 and CAT2/ Al_2O_3 corresponded to two copper oxide phases, CuO (JCPDS: 48-15-48) and Cu₂O (JCPDS: 77-01-99), indicating that the mixed oxide samples were composed of the two. The same goes for zinc oxide, cubic (JCPDS: 65-06-82) and hexagonal (JCPDS: 89-05-11) zinc oxide structures that appear only at alumina-supported catalysts (samples CAT1/ Al_2O_3 and CAT2/ Al_2O_3) with d-spacing values of 2.81, 2.47 and 1.62 Å for planes (100), (002) and (101) can be found in Table S2. Metallic copper with significant diffraction peaks at 43° (2θ) and 51° (2θ) with d-spacing values 2.01 Å and 1.81 Å (Table S3) can be found as well and it is further confirmed by EELS technique.

To compare the crystal structure of fresh and spent CAT2/ Al_2O_3 material, XRD analysis of the sample after catalytic testing was further performed. In Fig. S2 (Electronic Supplementary Information) the diffraction peaks with strong intensities for the used

**Fig. 1.** Powder XRD patterns of Cu-Zn catalysts.

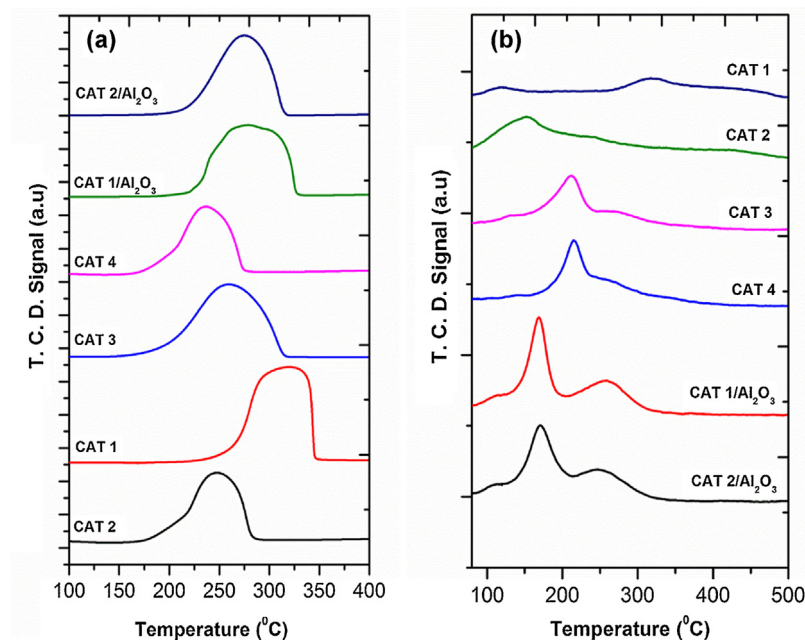


Fig. 2. H₂-TPR (a) and H₂-TPD (b) profiles of Cu-Zn catalysts.

sample (sample CAT2/Al₂O₃ spent) can be observed. Visible signals appear at the angles corresponding to (111) and (200) planes that appear due to the formation of metallic copper because of the reduction atmosphere [43]. Alumina contributions are still present and appear as more crystalline peaks than those of fresh sample; nonetheless, they overlay with the high-intensity above-mentioned peaks. Diffraction peak at 46° (2θ) could be assigned as γ-Al₂O₃ [44]. The formation of a sharp signal (at c. 51° (2θ)) that appears due to the presence of copper metal can be observed. The diffraction peaks of all analyzed samples are in good agreement with standard JCPDS cards of ZnO, CuO, Cu₂O, Cu and Al₂O₃ shown in Supplementary Information (Fig. S1).

To further clarify the distribution of the formed phases on the oxidized samples, SEM, TEM, XPS and energy-dispersive X-ray spectroscopy (EDXS) element mapping analyses were carried out.

The TPR profiles of the prepared catalysts are shown in Fig. 2. Jung and co-workers [45,46] indicated that ZnO reduces in the presence of methanol and CO, while with H₂ it does not below 600 °C. There are no peaks observed in the TPR profile of alumina was detected under the reduction conditions employed in this study. Thus, the peaks present in the TPR profile is due to the reduction of Cu/Zn phases in the catalyst. In the H₂-TPR profiles of Cu/Zn catalysts, it can be seen that there are two generalized convoluted TPR peaks, namely in the ranges of 150–280 °C and 230–350 °C. For the CAT2–CAT4 materials the low-temperature signal occurs slowly after 150 °C, while the position of the high-temperature reduction is shifted towards lower regions. As reported in the literature [9,47], the low-temperature peak in the TPR profiles can be attributed to the reduction of nanoparticles and the high temperature peak appear due to the large particles, originated from the bulk phase. Thus, in Fig. 2(a), the first peak (low temperature) is formed due to the reduction of isolated copper ions distributed on the catalyst surface while the second one (high temperature) from the small sized CuO nanoparticles [48].

The present results are in agreement with the metal dispersion, calculated using N₂O titration [49–51]. Besides pure CuO, the presence of Cu²⁺ species, included in mixed phases, was hypothesized, such as Cu-aluminate or Cu²⁺ ions, incorporated in the octahedral sites of Al₂O₃ or vicariant in zinc oxide or aluminate. These moieties should undergo the reduction at a temperature, higher than

that of CuO [50,52,53]. Some authors studied Cu/ZnO/Al₂O₃ catalysts and observed the TPR signals at much lower temperatures than those of bulk CuO, and attributed them to highly-dispersed CuO species [45,54]. Moreover, the low-temperature peaks, that are present in the profiles of both Cu/ZnO/Al₂O₃ materials, suggest that the application of Al₂O₃ will provide for the dispersion of the CuO phase. However, a direct quantitative relation between signal temperature and the content of the species in a precursor cannot be derived (e.g. Cu⁺/Cu²⁺ also influencing reduction, such as in CAT1). This suggests that other factors, such as the interaction with ZnO, can affect the reducibility of CuO [39,49,55]. No peaks for alumina were detected under the reduction conditions, employed in this study. Similar to Al₂O₃, ZnO reducibility was not observed in the applied temperature range.

The characteristic features of hydrogen desorption were determined by H₂-TPD, while the profiles of supports exhibited no H₂ evolution. The total amount detected was in the range of 0.32–0.37 μmol H₂/g for CAT1/Al₂O₃ and CAT2/Al₂O₃ catalysts. Quantitatively, the number and temperature of the peaks in the TPD profiles for both Al₂O₃-containing materials were similar. A representative response for Cu/Zn catalysts, in general, showed two peaks – in the range of 100–200 °C (Region I) and 200–400 °C (Region II). For CAT1/Al₂O₃ and CAT2/Al₂O₃, a high amount of H₂ was desorbed in the Region I with only some hydrogen evolved in the Region II. It was proposed that the high-temperature desorption is due to the presence of subsurface hydrogen, i.e. the one, present in a catalyst lattice, just below the surface of the copper atoms [56]. In addition, it was indicated that this evolution process results from the storage in the copper–alumina or zinc–alumina alloys formed [38,50,57]. Thus, the hydrogen, desorbed at a higher temperature, originates from strongly-chemisorbed and subsurface H₂, as well as and metal hydrides. Among the catalysts, both bimetallic copper–zinc materials showed a low amount of the H₂ desorption in all regions.

Weak, strong and some moderate acidic sites are attributed to the three peaks, present in the NH₃-TPD profile (Fig. 3a) of the prepared catalysts (Table 2), at 150–300 °C for weak acidic sites, at 300–600 °C for moderate acidic sites, and above 600 °C for strong acidic sites, respectively [58,59]. The latter are very well discussed in the literature [60–62] with the generation of an acidic site occur-

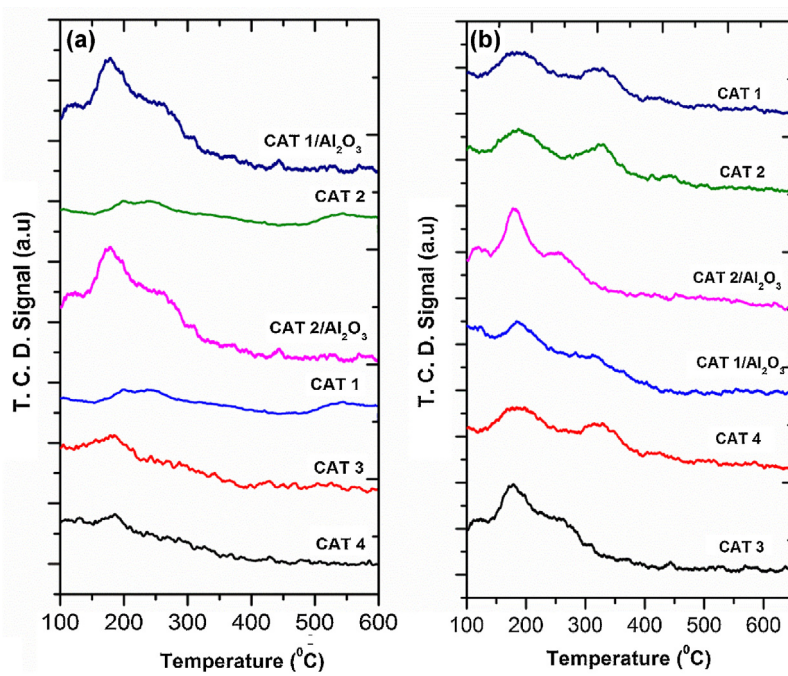


Fig. 3. NH₃-TPD (a) and CO₂-TPD (b) profiles of Cu-Zn catalysts.

Table 2

Distribution of acidic sites on prepared catalysts.

Catalyst	Acidic site distribution				Total acidity (μmol _{NH3} /g)
	Weak sites (μmol _{NH3} /g)	Moderate sites (μmol _{NH3} /g)	Strong sites (μmol _{NH3} /g)	Total acidity (μmol _{NH3} /g)	
CAT1	0.8	0.5	0.1	1.4	
CAT2	0.4	0.2	0.1	0.7	
CAT3	1.8	1.1	0.8	3.7	
CAT4	1.2	0.7	0.5	2.4	
CAT1/Al ₂ O ₃	2.1	1.2	1.1	4.4	
CAT2/Al ₂ O ₃	2.2	1.4	1.1	4.7	

ring when an oxide is deposited onto another to in turn form a surface-phase oxide. Thus, the acidity of copper in the presence of zinc and alumina was investigated for the synthesized catalysts. TPD studies using NH₃ revealed the presence of both the Lewis and Brønsted acidic sites. The Lewis acid sites have been shown to be generated by the deposition of zinc and alumina onto copper [63]. Conversely, the existence of the Brønsted acid sites has been demonstrated to occur when 3+ cations substitute into copper, only to produce a labile proton, bonded to the surface by ionic forces [39]. The second type of the Brønsted acidity (strong acidity) is produced by alumina, which forms electronegative cations. When compared to the catalysts, prepared by sol-gel method, the catalysts, synthesized through wet impregnation, showed a high acidity, which could be due to the high metal dispersion on the surface of these catalysts. The catalysts, containing a high amount of copper (i.e. CAT1), showed a high amount of weak acidic sites, while the catalysts, containing a high amount of zinc (i.e. CAT2), showed a low amount of the latter (Table 2). Among all the catalysts, both alumina-supported materials showed the highest total acidity, followed by the commercial alumina-doped analogues.

Furthermore, weak, strong and some moderate basic sites were ascribed to the three peaks, present in the CO₂ TPD profile (Fig. 3b) of the prepared catalysts (Table 3), namely the weak basic sites at 150–300 °C, the moderate basic sites at 300–600 °C, and the strong basic sites above 600 °C, correspondingly [59,64]. TPD studies using CO₂ revealed the presence of the Lewis and Brønsted basic sites

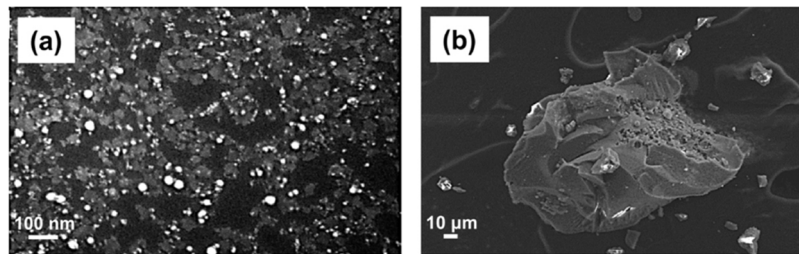
on the surface of the prepared catalysts. On the respective surface of the oxides of low oxidation state metals, metal-to-cation bond exhibits a highly ionic character, and thus, when this surface is crisp, the unsaturated metal cations are able to act as Lewis basic sites. The strength of these surface Lewis sites depends on the ionic character of the metal-to-cation oxygen bond, the ratio between the charge of the cation and its ionic radius, as well as its coordination [38,65]. Therefore, when a cation has a low charge and larger ionic radius (e.g. Zn), basicity predominates. In the oxides of semimetals such as alumina, the metal-to-oxygen bond is largely covalent, and thus, there is no coordinative unsaturation at the exposed surface, owing to surface –OH groups saturating coordination vacancy, thus resulting in Lewis basic sites [39,50]. The same trend was observed in the present study that is Lewis basic sites dominating in all the catalysts synthesized.

In general, alumina consists of weak basic sites, which are modified by the presence of Cu and Zn on the surface of the prepared catalysts. In multicomponent mixed oxides, a simpler situation is represented by the case, in which only two types of cations are present. When the two have similar oxidation states and electronegativity, the global acidic–alkaline characteristics are often dominated by those of one of the two components [32,66]. Thus, in the present case, the basic character of the catalysts is strongly pronounced by the presence of copper when compared to zinc and alumina.

Table 3

Distribution of basic sites on prepared catalysts.

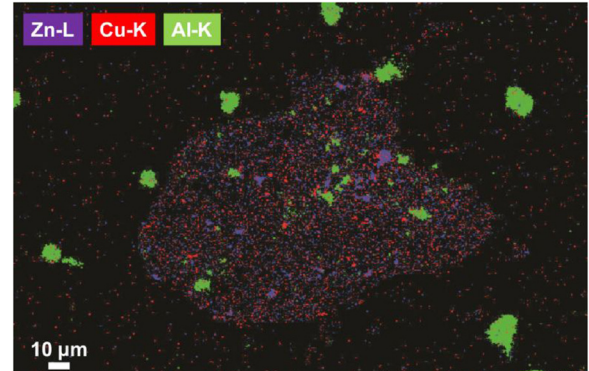
Catalyst	Basic site distribution			
	Weak sites ($\mu\text{mol}_{\text{CO}_2}/\text{g}$)	Moderate sites ($\mu\text{mol}_{\text{CO}_2}/\text{g}$)	Strong sites ($\mu\text{mol}_{\text{CO}_2}/\text{g}$)	Total basicity ($\mu\text{mol}_{\text{CO}_2}/\text{g}$)
CAT1	1.5	1.8	0.7	4.0
CAT2	1.4	1.2	1.1	3.7
CAT3	2.7	2.1	1.5	6.3
CAT4	2.9	2.5	1.9	7.3
CAT1/ Al_2O_3	3.7	2.4	1.4	7.5
CAT2/ Al_2O_3	4.2	2.1	1.2	7.5

**Fig. 4.** SEM images of CAT1/ Al_2O_3 catalyst.

The characteristic features of hydrogen desorption were foremost determined by the support (Al_2O_3) acidity (through metal dispersion) and reduction temperature; the H_2 -TPD profiles of the supports themselves revealed no hydrogen desorption. A representative H_2 -TPD profile for both alumina supported catalysts showed four desorption peaks in the respective ranges of 100–200 °C (Region I; metallic copper), 250–400 °C (Region II; intermetallic copper), 400–600 °C (Region III; the first subsurface layers), and above 600 °C (Region IV; the subsequent subsurface layers). A high amount of H_2 was desorbed in the Regions I and II with some of it being evolved in the Regions III and IV. The total hydrogen desorbed was in the range between 0.42 and 0.45 $\mu\text{mol H}_2/\text{g}$ for both the alumina-supported catalysts. Furthermore, the amount of hydrogen, desorbed in Region I, is higher than the one in other regions. It has been proposed that hydrogen, desorbed in high-temperature regions, appears due to the formation of subsurface hydrogen, i.e. hydrogen, present in catalyst lattice, just below the surface of copper atoms [56]. In addition, it has been outlined that high-temperature reduction results in the formation of copper–alumina or zinc–alumina alloys [38,50,57]. Thus, the evolved hydrogen, desorbed at a higher temperature, does not result from the copper with e.g. strongly-chemisorbed hydrogen, but rather from subsurface hydrogen and metal hydrides. From H_2 TPD results alongside with TPR profiles, it can be concluded that the majority of hydrogen results from desorption of the latter from copper, located on the support. Quantitatively, the number and characteristic temperatures of the peaks in the TPD profiles for both alumina supported catalysts are rather alike. Among catalysts, both sol–gel prepared zinc catalysts showed a low amount of the hydrogen desorption in all regions.

SEM images of the synthesized catalysts CAT1/ Al_2O_3 and CAT2/ Al_2O_3 are displayed in Figs. 4–6. Fig. 4a shows a uniform distribution of the sample CAT1/ Al_2O_3 . As indicated in Figs. 4 b and 6, the particles have a similar morphology even if the ratio of zinc and copper species is different. Since the mean atomic number of Cu–Zn compounds is higher than that of alumina, Cu–Zn nanoparticles in SEM images appear as a darker contrast in comparison with alumina particles.

The SEM/EDXS measurements (Figs. 5 and 6) of individual particles confirmed the presence of Cu–Zn alloy, as a consequence of the reduction of the catalyst at 400 °C using hydrogen. An oxide

**Fig. 5.** SEM/EDXS element mapping of modified Cu–Zn catalyst (CAT1/ Al_2O_3).

phase of Al_2O_3 on top of bimetallic Cu–Zn is also observed showing the uniform distribution of alumina particles on the sample surface. For the better understanding of element distribution separate SEM/EDXS maps of CAT1/ Al_2O_3 are provided in Supplementary Information (Fig. S3).

The observed morphology of the sample CAT2/ Al_2O_3 after catalytic testing (spent sample CAT2/ Al_2O_3) is shown in Fig. S4 (Electronic Supplementary Information) and it seems to be rather similar to the fresh modified sample CAT2/ Al_2O_3 . This was further confirmed by TEM analysis. The particle-size distribution of the spent sample was also investigated by SEM/EDXS mapping that confirmed the uniformly-distributed Cu, Zn and Al atoms (Fig. S4).

To investigate the structure and morphology of the fresh and spent sample CAT2/ Al_2O_3 in depth, TEM analysis was further performed (Fig. 7). From TEM micrographs, the round-shaped particles, ranging up to 7 nm in diameter, could be observed for both catalysts (Fig. 7a). Further, the average crystallite size was analyzed by Scherrer equation as well [67,68]. According to the Scherrer analysis, the average crystallite size of the fresh catalyst CAT2/ Al_2O_3 is smaller when compared to the used sample (sample CAT2/ Al_2O_3 spent) and is around 7 nm as observed with TEM analysis, too. The particle size after thermal reduction process increases and according to the Scherrer equation, the average crystallite size is around 25 nm. Since the calculated size of the crystallites is bigger than the particle size observed by HR-TEM (Fig. 7b), we presumed that after cat-

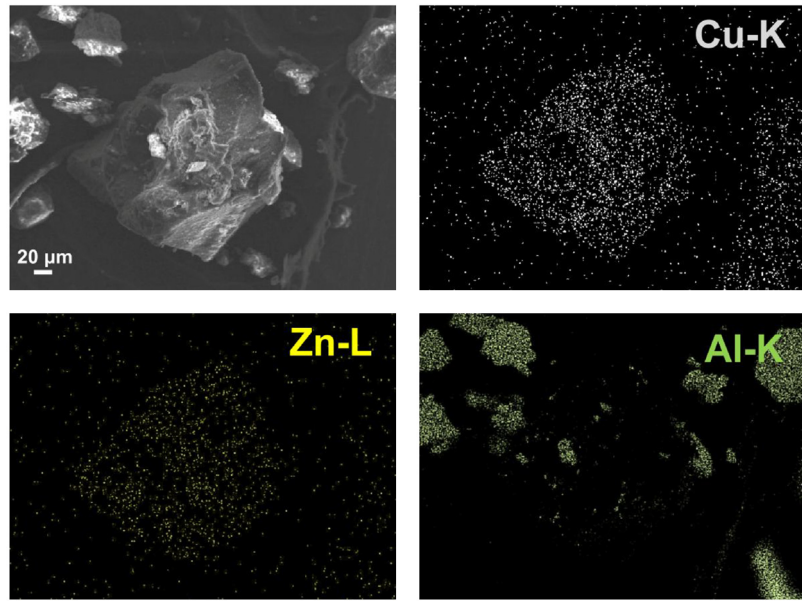


Fig. 6. SEM/EDXS element mapping of modified Cu–Zn catalyst (CAT2/Al₂O₃).

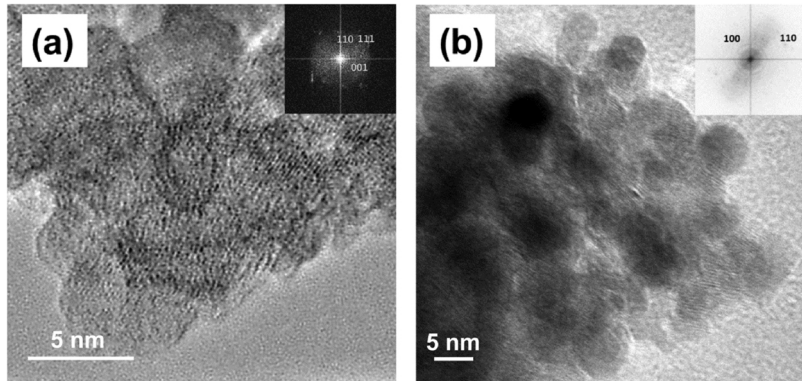


Fig. 7. TEM images of fresh (a) and spent (b) CAT2/Al₂O₃.

alytic testing some particles might agglomerate and the size could increase due to the agglomeration of copper active sites. Measuring the lattice fringes by high-resolution TEM (HR-TEM) images, it was confirmed for both catalysts that the said domains mainly comprised a cubic copper phase (Fig. 7a) as well as copper (I) oxide phase, was determined for used sample CAT2/Al₂O₃ confirming the (110) plane (Fig. 7b). Round shaped particles (especially nicely visible on Fig. 7b) that appear in darker contrast can be assigned as metallic copper. Due to the overlapping of Cu-Zn peaks is it hard to discuss identification and distribution of metal oxide particle.

However, besides pure Cu, areas containing Cu(I) oxide (Cu₂O) were also determined using EELS spectroscopy (Fig. S5 (Electronic Supplementary Information)). A relatively broad small white line at the beginning of Cu absorption edge (at 926 eV ($1 \text{ eV} = 1.60 \times 10^{-19} \text{ J}$)), characteristic for Cu(I), was noted. Beside Cu-, also oxygen edge (at 528 eV) was present in the case of oxides. From STEM/EDXS elemental mapping (Fig. S6 (Electronic Supplementary Information)), it was concluded that Zn was not uniformly distributed in samples; nonetheless, it was always appearing in combination with copper species.

The chemical states of material systems were further investigated by XPS. Fig. 8 shows the XPS spectra of the sample CAT2/Al₂O₃ after ammonia decomposition reactions (spent catalyst CAT2/Al₂O₃). The whole XPS survey profile of material surface

(Fig. 8a) presents all the elements detected. Since C (atmospheric), O, Cu, Zn and Al were detected, it could be surmised that metal oxides were formed in top layers. Fig. 8b reveals the de-convoluted XPS spectra of Cu 2p core level. The peak, located at approximately 932.6 eV, was attributed to the Cu 2p_{3/2} in Cu₂O. On the other hand, the signal with the binding energy of 934.6 eV was assigned to the Cu 2p_{3/2} in CuO. Meanwhile, an observation of a series of the satellite peaks at around 940.5 and 943.8 eV could be made for Cu 2p_{3/2} and Cu 2p_{1/2}, indicating the existence of an unfilled Cu 3d shell. All data were in good agreement with recently published reports [69].

Combining XPS, EDXS and XRD results, it could be concluded that both copper oxide phases were detected in the fresh as well in the spent CAT2/Al₂O₃ catalyst after catalytic testing, confirming the presence of the Cu⁺ and Cu²⁺ species in the said sample.

Fig. 9 shows NH₃ conversion as a function of temperature over the alumina-supported Cu- and Cu/ZnO-based catalysts. Clearly, NH₃ conversion increased with temperature, while the decomposition is in its essence endothermic ($\Delta H_r^{\theta\delta} = 46 \text{ kJ mol}^{-1}$). NH₃ consumption elevates (and levels for CAT1/Al₂O₃) upon applying the alumina substrate materials to a maximum of 92% which is below the thermodynamic equilibrium conversion at 600 °C, i.e. 100% (Table S4 (Electronic Supplementary Information)). On the other hand, neat Al₂O₃ support showed no significant conversion under the reaction conditions employed. Among all catalysts, both

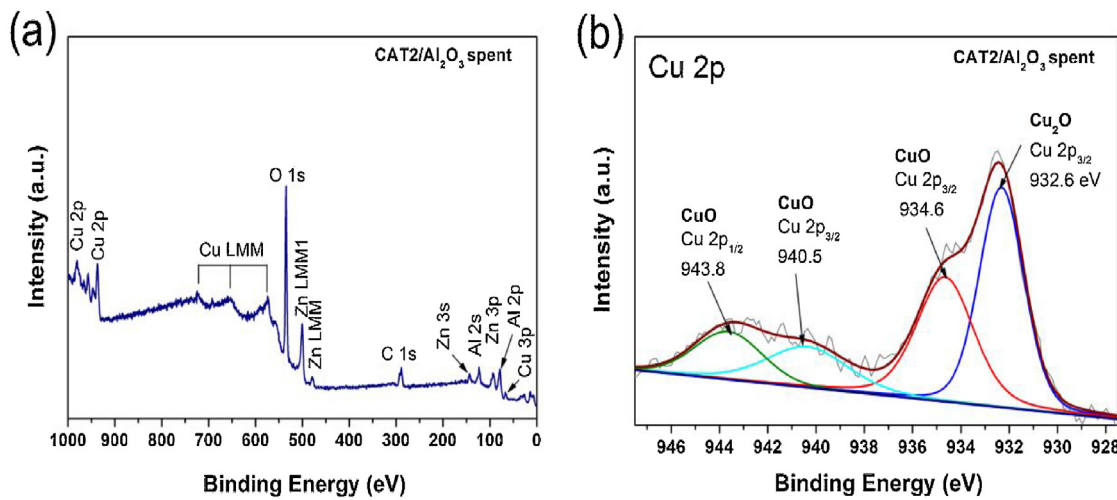


Fig. 8. XPS survey of CAT2/Al₂O₃ sample after catalytic testing (a) and high-resolution scans of Cu 2p core-level photoelectrons for CAT2/Al₂O₃ sample (b).

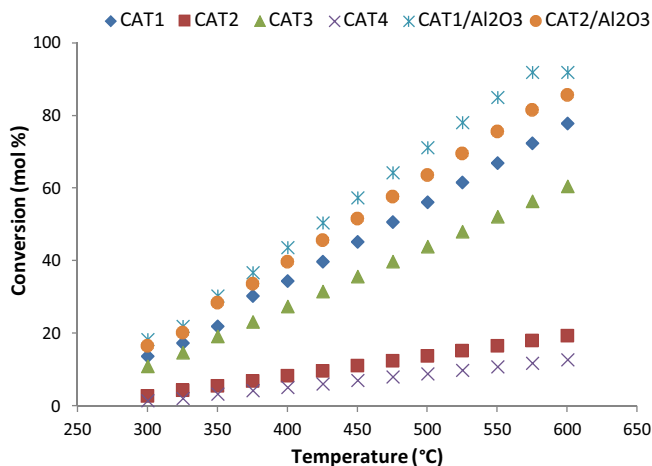


Fig. 9. Ammonia decomposition profiles of prepared catalysts.

CAT1 and CAT2 materials exhibited a very poor activity. This could be due to the low metal dispersion and meager reducibility of the zinc species on alumina. Both CAT3 and CAT4 catalysts granted a lower conversion when compared to Al₂O₃-supported analogues; this could be due to the synergistic effect of these binary materials (CAT1/Al₂O₃ and CAT2/Al₂O₃), containing well-dispersed Cu and Zn metals, present on their surface (Fig. 1). Both CAT1/Al₂O₃ and CAT2/Al₂O₃ catalysts attained 100% conversion at 700 °C with a higher hydrogen production rates with compared to other catalysts. Li and co-workers, as well as Zhang et al. [34,70], reported that bimetallic sites may be more active than their monometallic counterparts for ammonia decomposition. Thus, the dispersion of species, as well as the acidic and basic nature of a material played an important role, even more so than the presence of two (or several) metals on the surface of a catalyst. In overall, both alumina-supported samples exhibited a superior activity, which may be due to the synergistic effect for ammonia decomposition, a smaller average (nano)particle size of bimetallic, and the more moderate acid–base properties of support (Tables 1–3).

The NH₃ conversions over the synthesized catalysts remarkably increased as reaction temperature rose from 300 °C to 600 °C that is, over all materials. With ammonia decomposition being an apparent first-order reaction, the effective activation energy (E_a) of 73 ± 1 kJ/mol was estimated in between 450 and 600 °C for CAT2/Al₂O₃, which is in good agreement with the similar values,

Table 4
NH₃ decomposition activity over Cu–Zn catalysts at 600 °C.

Catalyst	Turnover frequency (mol _{NH3} s ⁻¹)	Hydrogen formation rate (mol _{H2} /(g _{cat} . h)) [*]
CAT1	7.3	0.011
CAT2	10.2	0.015
CAT3	18.6	0.028
CAT4	21.3	0.032
CAT1/Al ₂ O ₃	30.5	0.045
CAT2/Al ₂ O ₃	38.6	0.058

^{*}g_{cat} stands for the mass of the catalyst used in the reaction.

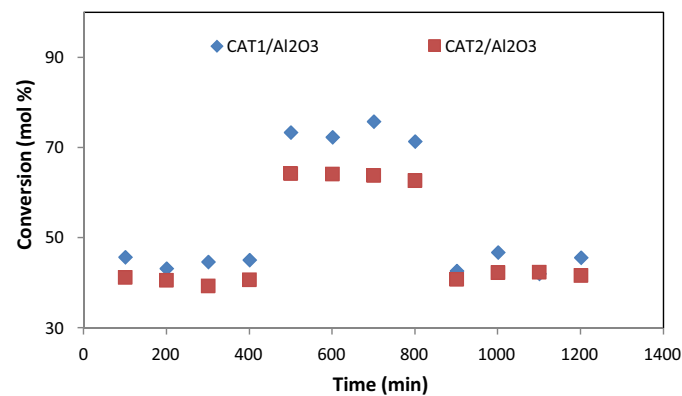


Fig. 10. Time-on stream conversion over CAT1/Al₂O₃ and CAT2/Al₂O₃ catalysts.

pertinent to other catalysts, employed for the same process. Similar E_a hint towards the presence of the same rate-determining step over copper materials. Furthermore, hydrogen formation rate was lower over the catalysts, prepared via the sol-gel method with regard to wet impregnation (Table 4). This is in agreement with H₂-TPD results, which revealed a high amount of the H₂ desorption at lower temperatures. Additionally, both alumina-supported catalysts were also characterized by the slightly higher activation energy for ammonia decomposition. This could be due to a highly basic character of the surface of these materials. As shown in Fig. 10, both alumina-supported catalysts do not show any loss in the NH₃ conversion under applied reaction conditions, indicating an excellent stability. The latter may be ascribed to the suppressing of the agglomeration by forming Cu–Zn bimetallic particles.

In literature, it is well established that bimetallic catalysts entail different chemical properties considering those of their indi-

vidual monometallic components, e.g. achieving the synergistic effects in ammonia decomposition reactions. In general, two-metal nitrides show a higher activity for NH₃ scission than their respective single-metal oxides. In some alumina-supported bimetallic systems (especially Co-Al, Fe-Al, Ni-Al and Co-Si) [12,29,71], the application of a thermal treatment or a high temperature can promote the reactions. On the other hand, at the temperature of 500 °C, Fe-Ni/Al₂O₃ and Fe-Mo/La₂O₃-Al₂O₃ exhibited a high hydrogen formation rates of 0.018 and 0.029 mol_{H2}/(g_{cat} h), respectively. The activity of Ni-Fe alloy was the highest when supported on alumina and Mg-Al spinel, if compared to SiO₂, TiO₂ and ZrO₂. Cu-Zn catalysts on γ-Al₂O₃ substrates, prepared in this study, demonstrated a high hydrogen formation rate when compared to other bimetallic systems, reported in the literature [12,14,72]. Several studies concur with regard to the synergistic effect in the poly-metallic systems, supported on alumina, which should be more active than the equivalent monometallic catalysts, e.g. containing Cu and Zn.

A requirement for bimetallic systems is a high stability under reaction conditions *versus* segregation into monometallic particles which would alter the surface properties and thus catalytic activity [73]. Additionally, in some supported bimetallic systems, the conditions of thermal treatment or high reaction temperatures can promote the formation of less reducible oxides such as Co-Al, Fe-Al, Ni-Al and Co-Si when supported on alumina or silica, resulting in considerably lower activity [10]. Several studies agree with the synergistic effect of the Co-Mo bimetallic system, supported on γ-Al₂O₃, to be more active than an equivalent monometallic Co or Mo catalysts [12,71]. The effect of the support on Co-Mo systems has also been studied by several authors with support-dependant activity following the trend of Al₂O₃ > MCM-41 > SiO₂ [15,72,74].

Monometallic Ru is highly active for the generation of CO_x-free H₂ from ammonia, and carbon nanotubes (CNT) are an excellent support material for such catalysts. The dispersion of Ru on CNT is the highest among all the other support materials examined in the literature [34,75]. A support of basic nature is required for high catalytic efficiency, and an increase in the support basicity leads to TOF enhancement of the Ru catalysts. The apparent activation energies of the reaction over Ru catalysts are dependent on the property of materials adopted as the catalyst support. N₂ desorption appears to be the rate-determining step in the catalytic NH₃ decomposition reaction. The results also implied that, if a support having both strong basicity and a good electronic conductivity is used with Ru catalyst, it will be possible to develop a more efficient catalyst for the generation of CO_x-free hydrogen from ammonia [76].

In general, the activity of catalysts in ammonia decomposition increases as the surface acidity and support surface area increases. The trend in activity may also be linked to alloy particle size, with Al₂O₃ and MCM-41 supports effectively stabilizing small sized particles [30]. The Cu-Zn particle size was also decreased when supported on Al₂O₃, showing a correlation between activity and particle size resulting from the choice of the support material. Support of this nature can be generated by proper design of novel composite materials. Also, optimization of catalytic performance can be achieved by fine-tuning the preparation procedures. The performance of the decomposition catalyst can be improved by increasing the dispersion of active component, as well as by eliminating the electron-withdrawing groups that originate from precursors of an active component, support or promoter. While platinum itself is not active for ammonia decomposition, theoretical studies show that when combined with nickel, iron or cobalt the binding energy increases from 418 kJ/mol, to just below the Ru (001) binding energy of 561 kJ/mol, suggesting that platinum could be effective in enhancing the activity of nickel, iron or cobalt [72,76]. Additionally, Cu, both in monometallic and bimetallic systems, is predicted to be inactive in this context [3,66]. Based on the catalytic results of bimetallic systems containing a sustainable

Table 5

Catalytic activity of ammonia decomposition for literature-reported bimetallic catalysts at 500 °C.

Catalyst	Turnover frequency (mol _{NH3} /s)	Hydrogen formation rate (mol _{H2} /(g _{cat} h))	Reference
Mo ₂ C	8.5	0.012	[4]
Cr ₂ O ₃	4.3	0.007	[34]
Fe-Ni/Al ₂ O ₃	10.8	0.021	[74]
Fe-Mo/La ₂ O ₃ -Al ₂ O ₃	11.8	0.029	[71]
Co-Mo/Al ₂ O ₃	14.8	0.021	[12]
Co-Fe/CNT	14.9	0.018	[77]
Ni-Pt/Al ₂ O ₃	17.5	0.034	[72]
Cu-Zn/Al ₂ O ₃	21.2	0.042	This work

metal substituent it is clear from the data presented in Table 5 that Cu-Zn is the most promising bimetallic candidate with the highest hydrogen rate reported at 500 °C.

4. Conclusions and outlook

Well-dispersed Cu-Zn catalysts on alumina have been prepared by modified citrate method. The catalytic activity of Cu-Zn catalysts increases with increase in copper loading and after supported on alumina. The dispersion of Cu species rose in the following order: CAT2/Al₂O₃ > CAT1/Al₂O₃ > CAT4 > CAT3. The catalysts with low zinc showed a lower dispersion compared to the copper analogue. From H₂ TPD results alongside with TPR profiles, it can be concluded that the majority of hydrogen results from desorption of the latter from copper, located on the support. Quantitatively, the number and characteristic temperatures of the peaks in the TPD profiles for both alumina supported catalysts are rather alike. A maximum ammonia conversion (92%) was observed over with a high copper content catalyst at 600 °C. In the present work, the catalysts showed a higher activity with compared to the other systems reported in the literature, could be ascribed to (i) a highly-active surface and the metal dispersion of Cu, (ii) an increase in the number of basic sites, and (iii) the enhancement of Cu-Zn interaction, which could effectively transfer the electrons between a metal and support. All the catalysts exhibited no loss in the NH₃ conversion activity under the applied reaction conditions, indicating that the materials have an excellent stability.

Acknowledgment

The authors gratefully acknowledge the financial support of the Ministry of Higher Education, Science and Technology of the Republic of Slovenia, and the Slovenian Research Agency (programs P1-0030, P2-0152 and P2-0393). The authors would also like to thank Dr. Janez Kovač for XPS measurements and discussions.

Appendix A. Supplementary data

Supplementary data associated with this article can be found, in the online version, at <http://dx.doi.org/10.1016/j.apcatb.2017.04.031>.

References

- [1] A. Klerke, C.H. Christensen, J.K. Norskov, T. Vegge, J. Mater. Chem. 18 (2008) 2304–2310.
- [2] Ammonia as a Hydrogen Source for Fuel Cells: A Review, Hydrogen Energy ? Challenges and Perspectives, in: Dragica Minic (Ed.), Open Access Publisher, 2012 (InTech, 10.5772/47759).
- [3] F. Schutth, R. Palkovits, R. Schlögl, D.S. Su, Energy Environ. Sci. 5 (2012) 6278–6289.
- [4] W. Zheng, T.P. Cotter, P. Kaghazchi, T. Jacob, B. Frank, K. Schlichte, W. Zhang, D.S. Su, F. Schutth, R. Schlögl, J. Am. Chem. Soc. 135 (2013) 3458–3464.
- [5] H. Inokawa, T. Ichikawa, H. Miyaoka, Appl. Catal., A: Gen. 491 (2015) 184–188.

- [6] F. Alhumaidan, D. Cresswell, A. Garforth, *Energy Fuels* 25 (2011) 4217–4234.
- [7] T.V. Choudhary, C. Sivadinarayana, D.W. Goodman, *Catal. Lett.* 72 (2001) 197–201.
- [8] R. Pelka, W. Arabczyk, *Chem. Pap.* 66 (2012) 18–25.
- [9] H. Silva, M.G. Nielsen, E.M. Fiordaliso, C.D. Damsgaard, C. Gundlach, T. Kasama, I.B. Chorkendorff, D. Chakraborty, *Appl. Catal., A: Gen.* 505 (2015) 548–556.
- [10] S.F. Yin, B.Q. Xu, X.P. Zhou, C.T. Au, *Appl. Catal. A: Gen.* 277 (2004) 1–9.
- [11] R. Metkemeijer, P. Achard, *Int. J. Hydrogen Energy* 19 (1994) 535–542.
- [12] J. Ji, X. Duan, G. Qian, X. Zhou, G. Tong, W. Yuan, *Int. J. Hydrogen Energy* 39 (2014) 12490–12498.
- [13] A. Boisen, S. Dahl, J.K. Nørskov, C.H. Christensen, *J. Catal.* 230 (2005) 309–312.
- [14] J. Zhang, H. Xu, X. Jin, Q. Ge, W. Li, *Appl. Catal. A: Gen.* 290 (2005) 87–96.
- [15] S. Podila, S.F. Zaman, H. Driss, Y.A. Alhamed, A.A. Al-Zahrani, L.A. Petrov, *Catal. Sci. Technol.* 6 (2016) 1496–1506.
- [16] S. Podila, Y.A. Alhamed, A.A. AlZahrani, L.A. Petrov, *Int. J. Hydrogen Energy* 40 (2015) 15411–15422.
- [17] X. Duan, G. Qian, X. Zhou, Z. Sui, D. Chen, W. Yuan, *Appl. Catal. B: Environ.* 101 (2011) 189–196.
- [18] S.F. Yin, B.Q. Xu, W.X. Zhu, C.F. Ng, X.P. Zhou, C.T. Au, *Catal. Today* 93–95 (2004) 27–38.
- [19] D.A. Hansgen, D.G. Vlachos, J.G. Chen, *Nat. Chem.* 2 (2010) 484–489.
- [20] Z.C. Orel, J. Maček, M. Marinšek, S. Pejovnik, *J. Eur. Ceram. Soc.* 27 (2007) 451–455.
- [21] P. Podbršček, Z.C. Orel, J. Maček, *Mater. Res. Bull.* 44 (2009) 1642–1646.
- [22] M. Zayat, D. Levy, *Chem. Mater.* 12 (2000) 2763–2769.
- [23] D. Segal, *J. Mater. Chem.* 7 (1997) 1297–1305.
- [24] C. Tisseraud, C. Comminges, T. Belin, H. Ahouari, A. Soualah, Y. Pouilloux, A. Le Valant, *J. Catal.* 330 (2015) 533–544.
- [25] A. Le Valant, C. Comminges, C. Tisseraud, C. Canaff, L. Pinard, Y. Pouilloux, *J. Catal.* 324 (2015) 41–49.
- [26] C. Wang, C. Liu, W. Fu, Z. Bao, J. Zhang, W. Ding, K. Chou, Q. Li, *Catal. Today* 263 (2016) 46–51.
- [27] H.-H. Tseng, H.-Y. Lin, Y.-F. Kuo, Y.-T. Su, *Chem. Eng. J.* 160 (2010) 13–19.
- [28] I.H. Tseng, W.-C. Chang, J.C.S. Wu, *Appl. Catal. B: Environ.* 37 (2002) 37–48.
- [29] H. Liu, H. Wang, J. Shen, Y. Sun, Z. Liu, *Appl. Catal. A: Gen.* 337 (2008) 138–147.
- [30] X.-K. Li, W.-J. Ji, J. Zhao, S.-J. Wang, C.-T. Au, *J. Catal.* 236 (2005) 181–189.
- [31] D.K. Bora, A. Braun, *RSC Adv.* 4 (2014) 23562–23570.
- [32] Z. Yuan, L. Wang, J. Wang, S. Xia, P. Chen, Z. Hou, X. Zheng, *Appl. Catal. B: Environ.* 101 (2011) 431–440.
- [33] W. Luo, F.-L. Jing, X.-P. Yu, S. Sun, S.-Z. Luo, W. Chu, *Catal. Lett.* 142 (2012) 492–500.
- [34] L. Li, Z.H. Zhu, S.B. Wang, X.D. Yao, Z.F. Yan, *J. Mol. Catal. A: Chem.* 304 (2009) 71–76.
- [35] S. Lenihan, T. Curtin, *Catal. Today* 145 (2009) 85–89.
- [36] H.G. Merkus, *Particle Size Measurements: Fundamentals, Practice, Quality*, Springer Science, Netherlands, 2009.
- [37] A.E. Aksyoju, J.L. Faria, M.F.R. Pereira, J.L. Figueiredo, P. Serp, J.C. Hierro, R. Feurer, Y. Kihn, P. Kalck, *Appl. Catal. A: Gen.* 243 (2003) 357–365.
- [38] A.T. Bell, *Science* 299 (2003) 1688–1691.
- [39] T. Shishido, M. Yamamoto, D. Li, Y. Tian, H. Morioka, M. Honda, T. Sano, K. Takehira, *Appl. Catal. A: Gen.* 303 (2006) 62–71.
- [40] P. Gao, F. Li, F. Xiao, N. Zhao, W. Wei, L. Zhong, Y. Sun, *Catal. Today* 194 (2012) 9–15.
- [41] Y. Zhang, L. Zhong, H. Wang, P. Gao, X. Li, S. Xiao, G. Ding, W. Wei, Y. Sun, *J. CO₂ Util.* 15 (2016) 72–82.
- [42] B.R. Jermy, B.P. Ajayi, B.A. Abusaud, S. Asaoka, S. Al-Khattaf, *J. Mol. Catal. A: Chem.* 400 (2015) 121–131.
- [43] D. Thi My Dung, L. Thi Thu Tuyet, F.-B. Eric, D. Mau Chien, *Adv. Nat. Sci: Nanosci. Nanotechnol.* 2 (2011) 025004.
- [44] J. Lian, J. Ma, X. Duan, T. Kim, H. Li, W. Zheng, *Chem. Commun.* 46 (2010) 2650–2652.
- [45] K.-D. Jung, O.-S. Joo, *Catal. Lett.* 84 (2002) 21–25.
- [46] K.-D. Jung, O.-S. Joo, S.-H. Han, *Catal. Lett.* 68 (2000) 49–54.
- [47] A. Gervasini, *Calorimetry and Thermal Methods in Catalysis*, in: A. Auroux (Ed.), Springer, Berlin Heidelberg Germany, 2013, pp. 175–195.
- [48] G. Córdoba, M. Viniegra, J.L.G. Fierro, J. Padilla, R. Arroyo, *J. Solid State Chem.* 138 (1998) 1–6.
- [49] M. Turco, G. Bagnasco, C. Cammarano, P. Senese, U. Costantino, M. Sisani, *Appl. Catal. B: Environ.* 77 (2007) 46–57.
- [50] F. Studt, M. Behrens, E.L. Kunke, N. Thomas, S. Zander, A. Tarasov, J. Schumann, E. Frei, J.B. Varley, F. Abild-Pedersen, J.K. Nørskov, R. Schlögl, *ChemCatChem* 7 (2015) 1105–1111.
- [51] J. Papavasiliou, G. Avgouropoulos, T. Ioannides, *Catal. Commun.* 6 (2005) 497–501.
- [52] G. Simson, E. Prasetyo, S. Reiner, O. Hinrichsen, *Appl. Catal. A: Gen.* 450 (2013) 1–12.
- [53] L. Chmielarz, M. Jabłońska, A. Strumiński, Z. Piwowarska, A. Wegrzyn, S. Witkowski, M. Michalik, *Appl. Catal. B: Environ.* 130–131 (2013) 152–162.
- [54] V. Durga Kumari, M. Subrahmanyam, A. Ratnamala, D. Venugopal, B. Srinivas, M.V. Phanikrishna Sharma, S.S. Madhavendra, B. Bikshapathi, K. Venkateswarlu, T. Krishnudu, K.B.S. Prasad, K.V. Raghavan, *Catal. Commun.* 3 (2002) 417–424.
- [55] Á. Mastalir, Á. Patzkó, B. Frank, R. Schomäcker, T. Ressler, R. Schlögl, *Catal. Commun.* 8 (2007) 1684–1690.
- [56] T. Chetty, H.B. Friedrich, V.D.B.C. Dasireddy, A. Govender, P.J. Mohlala, W. Barnard, *ChemCatChem* 6 (2014) 2384–2393.
- [57] R. Khoshbin, M. Haghghi, J. Nanosci. Nanotechnol. 13 (2013) 4996–5003.
- [58] V.D.B.C. Dasireddy, S. Singh, H.B. Friedrich, *Appl. Catal. A: Gen.* 456 (2013) 105–117.
- [59] H. Hattori, Y. Ono, *Solid Acid Catalysis: From Fundamentals to Applications*, Pan Stanford, CRC Press, Florida, United States, 2015.
- [60] J.R. Anderson, M. Boudart, *Catalysis: Science and Technology*, Springer-Verlag, Berlin, Germany, 1996.
- [61] G.V. Sagar, P.V.R. Rao, C.S. Srikanth, K.V.R. Chary, *J. Phys. Chem. B* 110 (2006) 13881–13888.
- [62] K.V.R. Chary, K.K. Seela, G.V. Sagar, B. Sreedhar, *J. Phys. Chem. B* 108 (2004) 658–663.
- [63] H. Lei, R. Nie, G. Wu, Z. Hou, *Fuel* 154 (2015) 161–166.
- [64] V.D.B.C. Dasireddy, S. Singh, H.B. Friedrich, *J. Mol. Catal. A: Chem.* 395 (2014) 398–408.
- [65] S. Nishimura, A. Takagaki, K. Ebitani, *Green Chem.* 15 (2013) 2026–2042.
- [66] M. Jabłońska, R. Palkovits, *Appl. Catal. B: Gen.* 181 (2016) 332–351.
- [67] L. Alexander, H.P. Klug, *J. Appl. Phys.* 21 (1950) 137–142.
- [68] M. Bitenc, M. Marinšek, Z. Crnjak Orel, *J. Eur. Ceram. Soc.* 28 (2008) 2915–2921.
- [69] P. Wang, Y.H. Ng, R. Amal, *Nanoscale* 5 (2013) 2952–2958.
- [70] L.-F. Zhang, M. Li, T.-Z. Ren, X. Liu, Z.-Y. Yuan, *Int. J. Hydrogen Energy* 40 (2015) 2648–2656.
- [71] B. Lorenzut, T. Montini, M. Bevilacqua, P. Fornasiero, *Appl. Catal. B: Environ.* 125 (2012) 409–417.
- [72] A.S. Chellappa, C.M. Fischer, W.J. Thomson, *Appl. Catal. A: Gen.* 227 (2002) 231–240.
- [73] G. Ertl, H. Knözinger, F. Schüth, J. Weitkamp, *Handbook of Heterogeneous Catalysis*, Wiley, New Jersey, United States, 2008 (8 Volumes).
- [74] S.B. Simonsen, D. Chakraborty, I. Chorkendorff, S. Appl. Catal. Dahl, A: Gen. 447–448 (2012) 22–31.
- [75] L. Li, Y. Wang, Z.P. Xu, Z. Zhu, *Appl. Catal. A: Gen.* 467 (2013) 246–252.
- [76] A.K. Hill, L. Torrente-Murciano, *Appl. Catal. B: Environ.* 172–173 (2015) 129–135.
- [77] J. Zhang, J.-O. Müller, W. Zheng, D. Wang, D. Su, R. Schlögl, *Nano Lett.* 8 (2008) 2738–2743.